ACS Editors' Choice

JACS
JOURNAL OF THE AMERICAN CHEMICAL SOCIETY

Communication

pubs.acs.org/JACS

Terms of Use

Self-Assembly of Tetrahedral CdSe Nanocrystals: Effective "Patchiness" via Anisotropic Steric Interaction

Michael A. Boles and Dmitri V. Talapin*

Department of Chemistry and James Franck Institute, University of Chicago, Chicago, Illinois 60637, United States

Supporting Information

ABSTRACT: Controlling the spontaneous organization of nanoscale objects remains a fundamental challenge of materials design. Here we present the first characterization of self-assembled superlattices (SLs) comprised of tetrahedral nanocrystal (NCs). We observe self-assembly of CdSe nanotetrahedra into an open structure (estimated space-filling fraction $\varphi \approx 0.59$) which has not been anticipated by many recent theoretical studies and simulations of tetrahedron packings. This finding highlights a gap in the understanding of the hierarchy of energy scales acting on colloidal NCs during self-assembly. We propose a strong dependence of ligand−ligand interaction potential on NC surface curvature. This effect favors spatial proximity of vertices in the dense colloidal crystal and may be considered an emergent "patchiness" acting through chemically identical ligand molecules.

Tetrahedron packing has been studied in depth theoretically and computationally for many years. Spurring a recent revival in interest, Conway and Torquato showed that 20 tetrahedra may be packed into an icosahedron and subsequent lattice packing of icosahedra can produce an arrangement of tetrahedra with $\varphi \approx 0.72$.[1] In 2008, by constructing an 18-tetrahedron cluster and finding a suitable lattice packing of clusters, Chen reported dense tetrahedron packing with $\varphi \approx 0.78$,[2] providing the first example of an arrangement of tetrahedra which fills space more densely than fcc packing of spheres ($\varphi \approx 0.74$). The following year, Haji−Akbari et al. used Monte Carlo simulations to compress a fluid of hard tetrahedra to a quasicrystalline solid phase with a packing density $\varphi \approx 0.82$ and made a new periodic structure with 82 particles per fundamental cell and density $\varphi \approx 0.85$.[3] The current record is claimed by a double dimer packing with four tetrahedra per fundamental cell and $\varphi \approx 0.86$.[4]

In parallel, a lot of work has been dedicated to understanding the packing behavior of various "imperfect" tetrahedra. Phase diagrams have been calculated for tetrahedral particles with various degrees of truncation,[5] for tetrahedrally truncated spheres,[6] and for tetrahedral "puffs".[7] Simulations of hard faceted particles inspired the conceptual development of "directional entropic forces" (DEFs) that guide the assembly of anisotropic particles toward structures with parallel facet alignment.[8] In contrast to enthalpic patchiness (arising from, for example, molecular patterning[9] or DNA functionalization[10]) DEFs promote local dense packing.

Despite progress in mathematical constructions of tetrahedron (and pseudo-tetrahedron) packings, there exist few experimental investigations of such packings. In one example, Jaoshvili et al. poured tetrahedral dice into containers and used volumetric measurement to determine random close packings of tetrahedra have density 0.76 ± 0.02.[11]

Several recent studies suggest that self-assembly of semiconductor (CdSe, PbSe, etc.) NCs into SLs is an entropy-driven process.[12] This approach treats NC assembly as a packing problem with entropic stabilization of dense ordered phases. Indeed, spherical NCs typically arrange themselves in fcc or hcp packings, the most dense arrangements (both $\varphi \approx 0.74$) possible for spheres.[13] The role of translational entropy in driving NC assemblies to most-dense configurations suggests that colloidal NCs might offer insight into the mathematical problem of finding dense arrangements of non-spherical objects. On the other hand, tailoring soft interactions between NCs may enable formation of structures not anticipated for hard objects.

In this work we study the self-assembly of tetrahedral CdSe nanocrystals. Following a recipe outlined by Liu et al.,[14] zinc blende phase CdSe tetrahedra were synthesized by reacting cadmium oleate with elemental selenium in ODE at 250 °C (Figure 1a). The tetrahedral NC shape results from NC growth

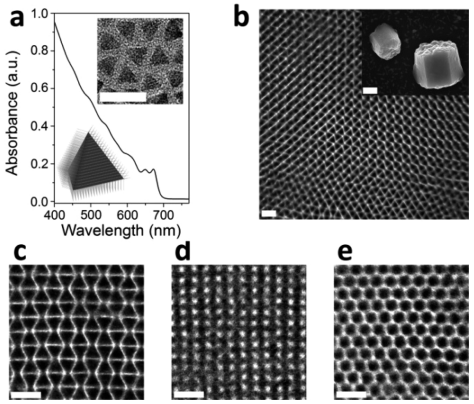

Figure 1. (a) Absorption spectrum of tetrahedral CdSe NCs in toluene with first peak at $\lambda = 670$ nm. Inset, top: TEM image of tetrahedral 10-nm CdSe NCs. Inset, bottom: model of 10-nm tetrahedron with C_{18}-length ligands. (b) TEM image of large-area superlattice. Inset: SEM image of hexagonal prism shaped three-dimensional crystals. (c−e) Close-up TEM images of three projections of the superlattice of CdSe NCs. TEM scale bars, 20 nm; SEM scale bar, 1 μm.

Received: February 14, 2014
Published: March 22, 2014

   dx.doi.org/10.1021/ja501596z | J. Am. Chem. Soc. 2014, 136, 5868−5871

occurring preferentially along (100) crystallographic directions due to the weaker binding of oleic acid ligands to the CdSe (100) surface than CdSe (111). The size and shape of CdSe NCs were confirmed by transmission electron microscopy (TEM) (Figure 1a, inset). Self-assembly was carried out by gentle evaporation of a colloidal solution of CdSe NCs in tetrachloroethylene over a TEM grid tilted at ~25° from horizontal.[15] CdSe tetrahedra readily assemble into SLs of μm^2-size dimensions (Figure 1b, S1) and frequently display twin boundaries (Figure S2). Here we emphasize that only one SL structure has been observed for CdSe nanotetrahedra with 8-nm and 10-nm edge length, capped with either oleic or stearic acid ligands (Figure S3), confirming the stability of this particular structure with respect to minor changes in NC size and ligand capping.

Three characteristic projections of the tetrahedron SL were observed: one revealing tetrahedra as equilateral triangles of alternating orientation (Figure 1c), another presenting a rectangular lattice (Figure 1d), and a third showing hexagonal arrangement of NCs (Figure 1e). Tilting experiments revealed these three arrangements are indeed different projections of the same crystal (Figure 2a).

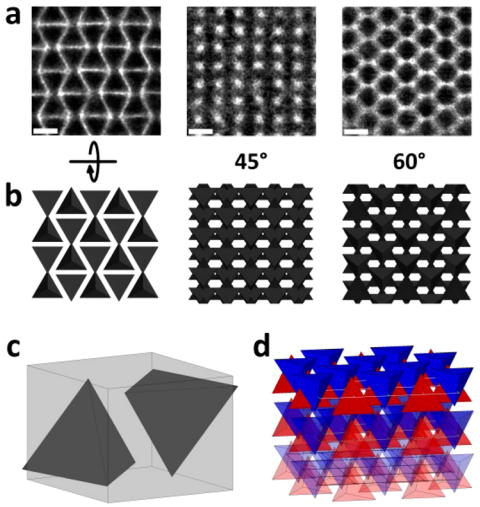

Figure 2. (a) TEM images of three projections of the superlattice. Scale bars, 10 nm. (b) Corresponding modeled superlattice projections. (c) Unit cell contains two tetrahedra in opposite orientations. (d) Superlattice structure after removal of surface ligands.

The SL of CdSe tetrahedra has a two-particle fundamental cell with tetrahedra in opposite orientations. It has C_{2h} $(2/m)$ symmetry with a center of inversion (Figure 2c). The SL can be reconstructed by placement of the inversion center of the dimer unit on the lattice points of a base-centered orthorhombic Bravais lattice (Figures 2d, S4). The lattice dimensions were estimated from particle tracking analysis of TEM images to be $a \approx 15.0$ nm, $b \approx 18.4$ nm, $c \approx 9.7$ nm (Figures S5,6). Projections of the modeled SL agree with the observed CdSe SL at tilt angles 0°, 45°, and 60° (Figure 2a,b).

Rather surprisingly, the SL structure shown in Figures 1 and 2 has not been observed in recent simulations, neither for ideal tetrahedra nor for their truncated or rounded "relatives". Also surprising is the fact that our structure cannot be rationalized as a dense packing of tetrahedra. While dense packings of convex polyhedra favor a large number of face-to-face contacts between particles, allowing particle centroids to be close to one another,[16] the distance between NC tetrahedron faces in our SL is estimated to be 5.1 ± 0.1 nm (Figure S7). This face-to-face separation is more than twice the extended length of oleic acid ligands (~2 nm) and thus precludes any contact between faces within the SL. Instead, the structure appears to be mechanically supported by vertex−vertex, face−vertex, and edge−edge contacts (Figure S8). In contrast, dense random close packings of tetrahedral dice investigated[11] by Chaikin et al. have on average ~2.5 face-to-face contacts per die, representing ~40% of all contacts between dice. No vertex-to-vertex contacts were observed for the dice. Similarly, mathematical constructions of dense tetrahedron packings reveal all four tetrahedron faces in contact with faces of neighboring tetrahedra.[1−4] The absence of face-to-face contacts and abundance of vertex-to-vertex contacts in the tetrahedral CdSe NC SL is reflected in the low packing density estimation.

The density of this SL might be estimated in one of two ways. If ligand shells are ignored, the tetrahedron crystal structure can be approximated by columns of tetrahedra in face-vertex contact (Figure S8). The volume fraction a tetrahedron occupies within its circumscribed triangular prism is approximately $\varphi \approx 0.33$. On the other hand, inclusion of ligands produces a space-filling estimate of $\varphi \approx 0.59$.[17] By this measure, our SL of tetrahedra is ~22% less dense than Chaikin's randomly-packed tetrahedral dice ($\varphi \approx 0.76$) and ~31% less dense than the current record (double dimer) packing ($\varphi \approx 0.86$) for perfect tetrahedra.

This observation of an open SL appears to contradict the widely accepted notion that semiconductor NCs should self-assemble into the (entropically favored) densest structure. It also suggests that recent simulations of entropy-driven tetrahedron packing[3,5−7] may be lacking some input parameters which play an important role during the self-assembly of real NCs. In fact, this observation of low-density NC SLs supported by vertex-to-vertex contacts is not the first of its kind: ~10-nm colloidal Pt_3Ni octahedra self-assemble into a low-density bcc structure (estimated space-filling factor of $\varphi \approx 0.48$ including oleylamine ligands) with exclusively vertex-to-vertex contacts[18] instead of, for example, the dense Minkowski packing of octahedra with $\varphi \approx 0.95$. In the remaining text we discuss effects which could lead to structures supported by vertex-to-vertex contacts instead of face-to-face contacts.

The soft potentials acting between NCs can either give rise to a new, low-density ground state of the system or lead to a specific assembly pathway followed by jamming of the SL structure at low density. Recent simulations by Geissler[19] and Glotzer[20] groups predict impressively complex ground states for soft spheres. Here we show that nonspherical soft NCs bring new complexity and new opportunities compared to their spherical counterparts.

Evolution of Particle Shape during the Assembly Process. Tetrahedral CdSe NCs used in this work are comprised of a core of CdSe, faces formed from Cd-terminated (111) facets, and a corona of oleic acid (OA) or stearic acid (SA) molecules covalently bound to surface Cd atoms. The inorganic core vertex radius of curvature is estimated to be on the order of ~0.5 nm from TEM images (Figure S10). The soft organic coating imparts a more significant perturbation to the tetrahedral NC shape. Since interaction between surface ligands is purely repulsive in the presence of good solvent such as tetrachloroethylene used in our assembly experiments,[21] ligand molecules can be expected to radiate isotropically from the tetrahedron surface when the NC is immersed in solution. The shape which best captures this effect is the tetrahedron "puff", which may be constructed from the overlap volume of four spheres placed at the vertices of a tetrahedron (Figure 3a). The perfect tetrahedron

dx.doi.org/10.1021/ja501596z | J. Am. Chem. Soc. 2014, 136, 5868−5871

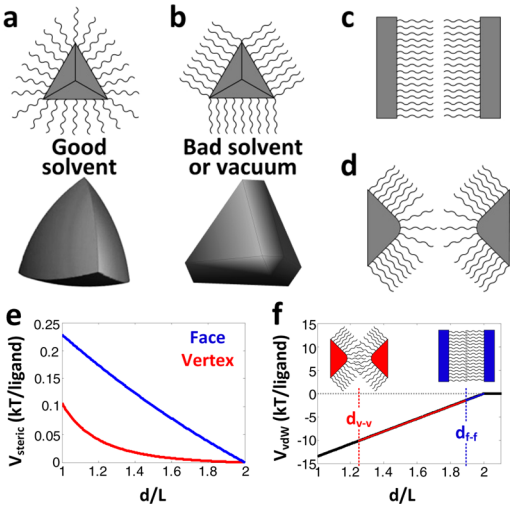

Figure 3. (a) Isotropic swelling of surface ligands in good solvent leads to "puffed" tetrahedron shape. (b) Bundling of ligands in the absence of solvent produces cantellated tetrahedron shape. (c) Sketch of ligand interaction between planar surfaces. (d) Sketch of ligand interaction between curved surfaces. (e) Calculated repulsive osmotic energy for a face-bound (blue) and vertex-bound (red) ligand at intermediate separation ($L \leq d < 2L$) in good solvent. (f) Calculated attractive van der Waals energy for two ligands in vacuum with interaction length determined by separation of grafting surfaces. The vertex−vertex separation distance measured in the superlattice is marked with the red trace; the blue trace position corresponds to a calculated equilibrium face−face distance based on the balance of vdW and elastic energies.[17]

has an asphericity ratio (the quotient of circumscribed and inscribed spheres, $\gamma = R_{out}/R_{in}$) of 3. Ligand molecules radiating from the tetrahedron surface will decrease the asphericity ratio, effectively rounding the shape of the NC. For a 2-nm fully extended ligand molecule[22] and 10-nm CdSe tetrahedron edge length, asphericity can be calculated as $\gamma = (R_{out} + L_{OA})/(R_{in} + L_{OA}) \approx 2$, where L_{OA} is the extended OA ligand length. Such puffs can approximate the physical shape of our CdSe NCs in a good solvent. On the other hand, interaction between ligands is strongly attractive in the absence of good solvent.[21] In later stages of the assembly process, when the carrier solvent is evaporated, the hydrocarbon tails of ligand molecules bundle together[23,24] to maximize van der Waals attraction. During solvent evaporation, the physical shape of tetrahedral CdSe-OA NCs evolves from a "puff' to a cantellated tetrahedron, whereby tetrahedron faces are translated outwards by an "effective" ligand length (Figure 3b). This type of shape evolution should be typical for all nonspherical particles.

Shape evolution may have important implications on the self-assembly pathway of tetrahedral CdSe NCs. For puffs with asphericity $\gamma = 2$, the densest packing was observed for a simple double lattice arrangement strikingly similar to our observed tetrahedral CdSe NC SL.[7] In addition, for $\gamma \approx 2$, packing of puffs reaches a local maximum, $\varphi \approx 0.83$, which may point to translational entropy as a significant factor prearranging puff-shaped CdSe NCs toward a colloidal crystal state that further evolves toward the SL structure shown in Figure 2a,b.

In addition to translational entropy, rotational entropy can play an important role in ensembles of nonspherical particles, generally favoring open lattice structures[25] which leave room for partial rotation of individual particles. For nonspherical particles, rotational entropy can also play a role in determining the pathway from dilute particle assembly to the final state of the SL. For example, a recent study[26] demonstrated the interplay between translational and rotational entropy for two-dimensional Brownian hard-square colloids, whereby compression causes the ensemble of squares to experience an order−order transition from a hexagonal rotator crystal to a rhombic phase which maximizes the sum of translational and rotational entropies of individual squares. In the case of faceted NCs, parallel facet alignment of face-to-face contacts will strongly suppress independent NC rotations, whereas vertex-to-vertex contacts do not restrict rotational degrees of freedom.

Anisotropic Steric Interactions. Anisotropic pair potentials imparted by "sticky patches" can control the ground state of particle assemblies.[27] The implied placement of ligand molecules with different chemical functionalities to form attractive interaction sites (patches), however, turned out to be a challenging synthetic problem.[8] Indeed, patchiness can be obtained by placement of the same ligand molecule at different locations on the NC surface: electrostatic patchiness has been demonstrated by Grzybowski et al., who showed with non-spherical metal NCs that local particle curvature influences the pH at which mercaptoundecanoic acid ligands are protonated.[28] Here we show that local surface curvature can significantly affect the pair potentials for even chemically identical ligand molecules.

In good solvent, hydrocarbon chains of ligands bound to the CdSe NC surface behave as a stretched polymer brush, imparting repulsive pair potentials to NCs and colloidal stability in nonpolar solvents. An osmotic term resulting from unfavorable exclusion of solvent molecules from the ligand interaction region acts upon the pair of particles as soon as their ligand coronas begin to overlap. This effect occurs during the whole range of steric interaction, beginning at interparticle distances lower than twice the width of the capping layer ($d < 2L$). Compression of the ligand chains results in an elastic contribution to the potential at smaller surface separations. Because this elastic component quickly exceeds thermal energy, the predominant region sampled during a Brownian collision is the moderate interpenetration ($L \leq d < 2L$) domain.[29] The steric potential onset may therefore be approximated by only the osmotic term: $V_{steric} \approx V_{osmotic}$.

Discussions[30] of steric stabilization of NCs have relied on theory developed for spherical polymer brushes[29] using the Derjaguin approximation. While this approach provides a good estimate for large particles ($R \gg L$), it significantly overestimates the strength of repulsion between particles whose radii and ligand length are similar ($R \approx L$).[31] To circumvent the shortcomings of traditional repulsion energy estimates for high-curvature geometries we employ the Flory−Krigbaum expression[32] for free energy of mixing of two chains tethered to surfaces 1 and 2 and brought together in volume dV starting from infinite separation: $V_{steric} = 2k_BT\cdot(\nu_s^2/\nu_i)\cdot((1/2) - \chi)\cdot\int_V \varphi_1\,\varphi_2\,dV$ where ν_s, ν_i, and χ are the Kuhn segment volume, solvent molecular volume, and Flory−Huggins chain−solvent interaction parameter, respectively. The segment density distribution functions φ_1, φ_2 are derived from the geometry of a cone-shaped available volume for ligands tethered to spheres.[17] For a ligand tethered to a high-curvature surface, the rapid decay of φ with increasing distance h from the surface leads to the small overlap integral $S_{12} = \int_{d-L}^{L} \hat{\varphi}_1\hat{\varphi}_2\,dh$ and small repulsive mixing energies. In the limit of $R \to \infty$, $\varphi(h) = $ const. for $0 < h \leq L$ and overlap integral S_{12} increases linearly with decreasing surface separation h.

For interaction between vertex ligands we calculated the mixing energy of two chains with rapidly decaying segment density distribution functions characteristic of the large conical

dx.doi.org/10.1021/ja501596z | J. Am. Chem. Soc. 2014, 136, 5868−5871

volume available to a ligand bound to a surface of high curvature. Here we used the estimated radius of curvature of the tetrahedron vertex, $R_{vertex} \approx 0.5$ nm. Interaction between tetrahedron faces was approximated with the estimated radius of curvature of the tetrahedron face $R_{face} \approx 15$ nm (Figure S11). Mixing energies per ligand for vertex−vertex and face−face interactions in good solvent in the moderate interpenetration domain ($L \leq d < 2L$) predict a much stronger repulsion between tetrahedron faces compared with tetrahedron vertices (Figure 3e). In the center of this region ($d/L = 1.5$ on the normalized abscissa), osmotic repulsion between face-bound ligands is predicted to be approximately an order of magnitude larger than that between vertex-bound ligands. Not considered in this analysis is the bending of ligands away from the contact axis, or "chain tilt", likely to occur in contacts between ligands tethered to highly curved surfaces and further reduce osmotic repulsion.[33]

The observed $\sim\mu m^2$-size domains for tetrahedron SLs suggest vertex-to-vertex contacts are sufficiently robust to prevent collapse of the low-density structure after solvent evaporation. The deep interpenetration of hydrocarbon chains bound to surfaces of high curvature may be responsible for this preservation of structural integrity. We estimated the vdW potential between two ligands in vacuum as a function of surface curvature and grafting surface separation using the expression given by Salem for interaction between long saturated hydrocarbon chains.[34] At a surface separation equal to the measured distance between tetrahedron vertices in the SL ($d_{v\text{-}v} \approx 2.5$ nm), we estimate a ligand vdW interaction strength of $\sim 10\ k_BT$ (Figure 3f, red trace). The ~5.1-nm separation measured between tetrahedron faces in the CdSe SL precludes contact between ligands. To estimate the interaction strength between face-bound ligands we used experimentally determined Young's modulus ($E \approx 1$ GPa) for C_{18}-length self-assembled monolayers[35] to construct a vacuum potential for face-bound ligands, incorporating attractive vdW and repulsive elastic components.[17] With a shallow minimum at $d_{f\text{-}f} \approx 3.75$ nm, the per-ligand vdW energy is predicted to be $\sim 1.5\ k_BT$ (Figure 3f, blue trace).

Both effects of strong repulsion per ligand between flat facets of tetrahedral NCs in good solvent and strong attraction per ligand between vertices of tetrahedral NCs in bad solvent or vacuum act to stabilize vertex-to-vertex contacts and penalize face-to-face contacts in the SL of CdSe tetrahedra. This observation may help to explain the prevalence of contacts between vertices of organic-capped nanotetrahedra investigated in this work and nanoctahedra explored by Smilgies and coworkers.[18] Incorporation of such an effect into thermodynamic simulations might represent a step towards the merging of theoretically-predicted and experimentally-observed packings of anisotropic nanoparticles which is needed to transform NC self-assembly into a powerful and predictable method for materials design.

■ ASSOCIATED CONTENT

Supporting Information

TEM images, superlattice modeling, measurements of interparticle separations, and calculation of ligand potentials. This material is available free of charge via the Internet at http://pubs.acs.org.

■ AUTHOR INFORMATION

Corresponding Author

dvtalapin@uchicago.edu

Notes

The authors declare no competing financial interest.

■ ACKNOWLEDGMENTS

We thank M. I. Bodnarchuk for early experiments on tetrahedron self-assembly and W. T. M. Irvine and E. R. Dufresne for the particle tracking code. This work was supported by the NSF MRSEC Program under Award No. DMR-0213745, by the David and Lucile Packard Foundation, and by the W. M. Keck Foundation.

■ REFERENCES

(1) Conway, J. H.; Torquato, S. *Proc. Natl. Acad. Sci. U.S.A.* **2006**, *103*, 10612.
(2) Chen, E. *Discrete Comput. Geom.* **2008**, *40*, 214.
(3) Haji-Akbari, A.; Engel, M.; Keys, A. S.; Zheng, X.; Petschek, R. G.; Palffy-Muhoray, P.; Glotzer, S. C. *Nature* **2009**, *462*, 773.
(4) Chen, E. R.; Engel, M.; Glotzer, S. C. *Discrete Comput. Geom.* **2010**, *44*, 253.
(5) Damasceno, P. F.; Engel, M.; Glotzer, S. C. *ACS Nano* **2011**, *6*, 609.
(6) van Anders, G.; Ahmed, N. K.; Smith, R.; Engel, M.; Glotzer, S. C. *ACS Nano* **2013**, *8*, 931.
(7) Kallus, Y.; Elser, V. *Phys. Rev. E* **2011**, *83*, 036703.
(8) van Anders, G.; Ahmed, N. K.; Klotsa, D.; Engel, M.; Glotzer, S. C. *arXiv:1309.1187*, **2013**.
(9) Chen, Q.; Bae, S. C.; Granick, S. *Nature* **2011**, *469*, 381.
(10) Wang, Y.; Wang, Y.; Breed, D. R.; Manoharan, V. N.; Feng, L.; Hollingsworth, A. D.; Weck, M.; Pine, D. J. *Nature* **2012**, *491*, 51.
(11) Jaoshvili, A.; Esakia, A.; Porrati, M.; Chaikin, P. M. *Phys. Rev. Lett.* **2010**, *104*, 185501.
(12) Evers, W. H.; Nijs, B. D.; Filion, L.; Castillo, S.; Dijkstra, M.; Vanmaekelbergh, D. *Nano Lett.* **2010**, *10*, 4235.
(13) Talapin, D. V. *ACS Nano* **2008**, *2*, 1097.
(14) Liu, L.; Zhuang, Z.; Xie, T.; Wang, Y.-G.; Li, J.; Peng, Q.; Li, Y. *J. Am. Chem. Soc.* **2009**, *131*, 16423.
(15) Bodnarchuk, M. I.; Kovalenko, M. V.; Heiss, W.; Talapin, D. V. *J. Am. Chem. Soc.* **2010**, *132*, 11967.
(16) Torquato, S.; Jiao, Y. *Phys. Rev. E* **2012**, *86*, 011102.
(17) Details available in Supporting Information.
(18) Zhang, J.; Luo, Z.; Quan, Z.; Wang, Y.; Kumbhar, A.; Smilgies, D.-M.; Fang, J. *Nano Lett.* **2011**, *11*, 2912.
(19) Gruenwald, M.; Geissler, P. *arXiv:1310.0652*, **2013**.
(20) Keys, A. S.; Glotzer, S. C. *Phys. Rev. Lett.* **2007**, *99*, 235503.
(21) Schapotschnikow, P.; Pool, R.; Vlugt, T. J. H. *Nano Lett.* **2008**, *8*, 2930.
(22) Mourdikoudis, S.; Liz-Marzán, L. M. *Chem. Mater.* **2013**, *25*, 1465.
(23) Widmer-Cooper, A.; Geissler, P. *Nano Lett.* **2013**, *14*, 57.
(24) Wang, Z. L.; Harfenist, S. A.; Whetten, R. L.; Bentley, J.; Evans, N. D. *J. Phys. Chem. B* **1998**, *102*, 3068.
(25) Mao, X.; Chen, Q.; Granick, S. *Nat. Mater.* **2013**, *12*, 217.
(26) Zhao, K.; Bruinsma, R.; Mason, T. G. *Proc. Natl. Acad. Sci. U.S.A.* **2011**, *108*, 2684.
(27) Zhang; Glotzer, S. C. *Nano Lett.* **2004**, *4*, 1407.
(28) Walker, D. A.; Leitsch, E. K.; Nap, R. J.; Szleifer, I.; Grzybowski, B. A. *Nat. Nanotechnol.* **2013**, *8*, 676.
(29) Vincent, B.; Edwards, J.; Emmett, S.; Jones, A. *Colloids Surf.* **1986**, *18*, 261.
(30) Saunders, A. E.; Korgel, B. A. *J. Phys. Chem. B* **2004**, *108*, 16732.
(31) Kim, J. U.; Matsen, M. W. *Macromolecules* **2008**, *41*, 4435.
(32) Napper, D. H. *J. Colloid Interface Sci.* **1977**, *58*, 390.
(33) Matsen, M. W. *Macromolecules* **2005**, *38*, 4525.
(34) Salem, L. *J. Chem. Phys.* **1962**, *37*, 2100.
(35) DelRio, F. W.; Cherno, J.; Fischer, D. A.; Cook, R. F. *Appl. Phys. Lett.* **2009**, *94*, 131909.